Fuel 235 (2019) 1275–1286

Contents lists available at ScienceDirect

Fuel

journal homepage: www.elsevier.com/locate/fuel

Full Length Article

Second-order gas slippage model for the Klinkenberg effect of multicomponent gas at finite Knudsen numbers up to 1

Shihao Wang[a,*], Alexander A. Lukyanov[b], Yu-Shu Wu[a]

[a] Petroleum Engineering Department, Colorado School of Mines, Golden, CO 80401, USA
[b] Havard Medical School, Boston, MA 02115, USA

ARTICLE INFO

Keywords:
Klinkenberg effect
Unconventional gas formation
Multicomponent gas
Non-empirical correlation
Kinetic theory of gases

ABSTRACT

Within microchannels, rarefied gas molecules frequently interact with the channel wall, resulting in non-zero velocity at the wall. This phenomenon is known as the gas slippage effect or Klinkenberg effect in porous media. Although the gas slippage effect of single component gas has been thoroughly investigated, an accurate correlation to account for the gas slippage effect in multicomponent gas flow has not been formulated so far. In this paper, we aim to quantify the multicomponent gas slippage effect by deriving a non-empirical second-order correlation.

Our approach is based on kinetic theory. We calculate the mean free path of gas mixtures, and capture the loss of horizontal flux momentum of gas flux after the molecules diffusively reflect at the wall. The horizontal flux momentum acts as shear stress on gas flow. In this sense, the loss of momentum induces reduction of viscosity and enhancement of mass transfer. By quantifying the loss of horizontal momentum as well as the reduction of viscosity, we can solve the gas slippage coefficient for the multicomponent gas flow system.

Our model captures the mass transfer mechanism of gas mixtures at low pressure (near-ideal condition). The accuracy of our model has been validated by both molecular-level simulation data and physical experimental data. The difference between our results and benchmark data is within 10% for Knudsen number up to 1.

Our model can be readily applied to the numerical simulation of unconventional gas formations.

1. Introduction

As discovered by Maxwell [1], when gas flows through narrow channels, the mass transfer rate increases due to momentum loss on the wall of the channel. In the micro scale, the gas becomes rarefied, and Navier-Stokes equation that is based on continuous assumptions is no more valid [2]. In this sense, the gas flow should be investigated from a kinetic viewpoint [3,4], and Boltzmann equation [5] should be adopted.

In the rarefied gases, the average distance that a gas molecular can move without any collisions is defined as the mean free path. The ratio between the mean free path and the flow channel diameter is defined as the Knudsen number, which is for the quantification of the magnitude of the gas-wall interaction effect. The gas-wall interaction results in the enhancement of mass transfer rate and is observed as an 'apparent' boundary slippage phenomena. Maxwell [1] brought out the very first slippage boundary condition, as shown in Eq. (1)

$$u_{slip} = \frac{2-\sigma}{\sigma}\cdot\lambda\left(\frac{\partial u}{\partial n}\right)_s \tag{1}$$

In this equation, u is the flux velocity at the boundary, σ is the Tangential Momentum Accommodation Coefficient (TMAC), which quantifies the ratio of momentum transfer on the boundary and λ is the mean free path of the gas. n denotes normal direction and s denotes (flat) surface. The detailed explanations of symbols used in this paper can be found in the Nomenclature list. A general form of the slippage boundary condition can be expressed as

$$u_{slip} = C_1(K_N)\cdot\lambda\left(\frac{\partial u}{\partial n}\right)_s - C_2(K_N)\cdot\lambda^2\left(\frac{\partial^2 u}{\partial n^2}\right)_s \tag{2}$$

As shown in Eq. (2) the boundary slippage velocity is a multiple order function of the velocity gradient. In Eq. (2), the term C_1 and C_2 are the coefficients of first-order velocity gradient and second-order velocity gradient, respectively. By comparing Eqs. (1) and (2), it can be

* Corresponding author.
E-mail address: shiwang@mines.edu (S. Wang).

https://doi.org/10.1016/j.fuel.2018.08.113
Received 26 June 2018; Received in revised form 17 August 2018; Accepted 24 August 2018
Available online 05 September 2018

Nomenclature

b	Klinkenberg factor
C	slippage coefficient
D	pore diameter
E_i	exponential integral function
i	component index
j	component index
k_B	Boltzmann constant
K_∞	absolute permeability
K_a	apparent permeability
K_N	Knudsen number
M_1	momentum transported by Type 1 molecules
M_2	momentum transported by Type 2 molecules
M_u	momentum transported by molecules from above
M_b	momentum transported by molecules from below
M	molecular weight
n_t	total number density
N	number of molecules
Q_D	dimensionless flow rate
P	pressure
R	gas constant
S	flow rate enhancement factor
T	temperature
δ	collision (kinetic) diameter
u	flux velocity
τ	unit volume
V	thermal velocity
x	horizontal dimension
x_i	mole fraction of ith component
z	vertical dimension
φ	spherical angle
ω	radial angle
λ	mean free path
ρ	density
σ	Tangential Momentum Accommodation Coefficient (TMAC)

seen that Maxwell's slippage boundary condition is a first-order boundary condition with a constant coefficient.

In the petroleum industry, gas slippage effect exists in the flow of gas through the pores of unconventional formation rocks which rang from several nanometers to several micrometers. Klinkenberg firstly discovered that the apparent gas permeability K_a could be larger than absolute rock permeability K_∞ and brought out a general model to quantify such effect, which was later named after him, as shown in Eq. (3).

$$K_a = K_\infty\left(1 + \frac{b}{P}\right) \tag{3}$$

In the above equation, b is an empirical parameter. Since $\lambda \propto 1/P$, Klinkenberg's correlation can be viewed as an empirical first-order slippage model.

Knudsen [6,7] investigated the diffusion effect induced by molecular-wall interaction for high Knudsen numbers and brought out the Knudsen diffusion effect along with the Knudsen diffusion coefficient. Pollard and Present [8] later studied the gas diffusion process in a long channel. According to Pollard and Present [7]'s model, Knudsen diffusion coefficient is the 'extreme' value for very high Knudsen numbers (extremely narrow flow channel). The diffusion coefficient decreases from Knudsen diffusion coefficient continuously to molecular diffusion coefficient as the Knudsen number decreases from infinitely large to infinitely small. Recently, the impact of surface geometry on Knudsen diffusion has also been investigated [9].

Rarefied gas flow and its associated gas slippage model has a wide range of applications in vacuum science [10], the design of microfluidics [11,12], aerospace engineering [13], microelectromechanical systems (MEMS) [14,15] and unconventional gas formations [16–21]. To simulate the rarefied gas flow, many numerical approaches have been proposed and applied. Direct Simulation Monte Carlo (DSMC) [22–26] directly tracks the motion of molecules. In this way, DSMC is able to obtain accurate results. DSMC has been used to obtain slippage boundary conditions [27] and to study the flow inside microchannels [28]. The limitation of DSMC is also obvious, that it is in need of huge computational capability.

Lattice Boltzmann Method (LBM) ([29,30]) solves Boltzmann equation on a grid-like lattice. LBM has been successfully applied to 'mesoscale' microfluid simulation for low to moderately high Knudsen number [31–33]. However, it should be noticed that LBM itself still requires a slippage boundary condition [34].

DSBGK method (direct simulation based on Bhatnagar–Gross–Krook equation) [35] is a promising method for rarefied gas dynamics. Compared to DSMC, DSBGK is less computationally consuming. Li [36] adopted DSBGK method to study the Klinkenberg effect with a two-dimensional digital rock and benchmarked against the traditional empirical Klinkenberg's correlation.

Gas kinetic scheme [37–39] is another appealing approach to numerically simulate the rarefied gas flow. Ohwada and Xu [40] combined gas-kinetic scheme with Burnett equation (a higher order approach [4]) to solve for the velocity profile as well as pressure/temperature distribution of gas flow inside microchannels.

Besides Burnett equation, numerous higher order continuum hydrodynamics approaches, including super-Burnett equation [41], Eu's generalized hydrodynamics approach [42], BGK-Burnett equation [43], 13-moment approach [44] and many more, have been proposed and studied. However, as pointed out by Lockerby et al. [45], these approaches may have instabilities and in general fail to match DSMC results well.

In recent years, more physical factors have been taken into the consideration of numerical approaches, such as the surface geometry [9,46], and the near-surface viscosity effect [47]. The flow in unconventional oil/gas formations is typically under high-temperature high-pressure conditions [48]. Moreover, in shale/clay reservoirs, when hydrogen molecules flow through the micro/nano scale channels in kerogen, the surface of the kerogen (as organic matter) has certain preference to gas components, which leads to the surface preference effect [28,49] as well as gas adsorption/desorption processes. Therefore, the slippage model in unconventional formations involves more complex multiphysical processes, including the surface diffusion in the adsorption layer [50], the impact of the pore-network geometry [51], the impact of the surface roughness [51], the real (dense) gas effect [52,53], the mechanical impact [54] and so on. Song et al. [55] brought out a comprehensive model for the calculation of gas apparent permeability of shale by considering stress effect, slippage effect and surface diffusion effect. Song's model can also be combined with our proposed model. The pore-network geometry of unconventional formations can be re-constructed by digital rock techniques. Yang et al. [56] brought out a novel approach to characterize the pore space geometry, in which the inorganic pore digital core and the organic pore digital core is constructed by the multiple point statistics method, and the Markov chain Monte Carlo method respectively.

As discussed above, the slippage boundary condition is of great importance in the quantification of rarefied gas flow. During the past years, numerous boundary conditions, including first order and second order condition, have been proposed. Among the proposed formulation, some representative models are as follows. Cercigani [57] derived a

second order boundary condition from the linearized Boltzmann equation. This boundary condition was later validated by Hadjiconstantinou [58]. Beskok and Karniadakis [59] proposed an empirical correlation to quantify the flow within multiple geometries for a wide range of Knudsen numbers. Wu and Bogy [60] used gas kinetic theory to address this problem and derived a simple yet accurate second-order model for relatively low Knudsen numbers that is below 1. They investigated the momentum loss on the pore wall with the kinetic theory of gases. Their model was later extended to higher Knudsen numbers [61]. Zhang et al. [62] and Wang et al. [63] have conducted thorough reviews and comparisons on the slippage effect and Klinkenberg phenomena respectively. From their observation, Wu [61]'s model is the most accurate non-empirical slippage boundary condition. Recently, Wang et al. [64,65] presented a novel second-order slippage model, which accurately calculates the mass transfer enhancement in microchannels and matches the numerical results [66] as well as physical experiment [67] data very well.

As for the slippage model for multiple component gas mixtures, Loyalka [68], Naris et al. [69], Takata [70], Garcia et al. [71] and Sharipov et al. [72–76] have studied the slippage of binary gas mixtures by solving the linearized Boltzmann equation. Hyakutake et al. [77] and Arcidiacono et al. [78] conducts DSMC simulation and LBM simulation for binary gas mixtures. Bentz et al. [79] and conducts Yamaguchi et al. [80] conducts spinning rotor gauge experiments and tube flooding experiments respectively to measure the slippage coefficient of binary gas mixtures.

As can be seen from the above literature review, although the slippage model of single component gas flow has been investigated in-depth, the non-empirical slippage model for multicomponent gas mixtures, however, has not been well developed yet. In this work, we proposed a non-empirical gas slippage for multicomponent gas mixtures. Our work is based on the published research [60,61,64,65] about single component gas slippage.

This paper is organized as follows. In Section 2, we briefly introduce the background of the kinetic theory of gases. In Section 3, we present the derivation of the proposed slippage model. In Section 4, we show the mass transfer enhancement factor predicted by our model. In the last Section, we conclude this work and suggest for future work.

2. Background

2.1. Mean free path of near-ideal gas mixture

By definition, the mean free path is the 'average' distance that a gas molecule can travel before it hits another gas molecule. The mean free path of gas can be calculated in several ways, resulting in slightly different values [3,4,24]. In this work, we follow Kennard's method [81] to calculate the mean free path of the ith component in a gas mixture with N_C components as follows

$$\lambda_i = \frac{4k_B T}{\pi P \sum_{j=1}^{N_C} n_j (\delta_i + \delta_j)^2 (1 + m_i/m_j)^{1/2}} \tag{4}$$

In the above equation, n_i is the number density of the ith type of molecules. δ_i and m_i is the collision diameter (kinetic diameter) and molecular weight of the ith type of molecules respectively. k_B and T is the Boltzmann constant and temperature respectively.

The 'average' mean free path of the gas mixture can be defined as

$$\lambda_{fm} = \sum_{j=1}^{Nc} x_j \lambda_j \tag{5}$$

Here λ_{fm} is calculated via a simple mixing rule and is used only for the calculation of Knudsen number to make comparison easier. From λ_{fm}, we can define Knudsen number for gas mixture as

$$K_N = \frac{\lambda_{fm}}{d} \tag{6}$$

In our work, we will use the above Knudsen number to calculate the mass rate enhancement factor of the gas slippage model. It should be pointed out that the above definition of Knudsen number is only for convenience (to be consistent with the formulation of single-component gases). It does not affect our derivation.

2.2. Diffusive reflection and momentum loss

The impinging molecules reflect on the wall of the porous media. A certain amount of reflections are specular, in which the molecules maintain their horizontal momentum. The rest of the molecules diffusively reflect into a random direction, causing a loss of momentum, as shown in Fig. 1. The diffusive reflection can be analogous to light scattering on rough surfaces and can be quantified by the method proposed by Bennett and Porteus [82], Davies [83] and Harvey et al. [84]. The percentage of the loss of the momentum is defined as Tangential Momentum Accommodation Coefficient (TMAC), ranging from *0* to *1*. The rougher the surface is, the higher the TMAC is.

The diffusively reflected molecules will lose their horizontal momentum after the reflection. Since the momentum gradient is the origin of shear stress, the loss of horizontal momentum will reduce the shear stress and thus reduce the viscosity of fluid that is in the vicinity of the pore wall, causing the fluid to 'slip.' In this work, we aim to quantify the slippage effect by quantifying the amount of lost momentum.

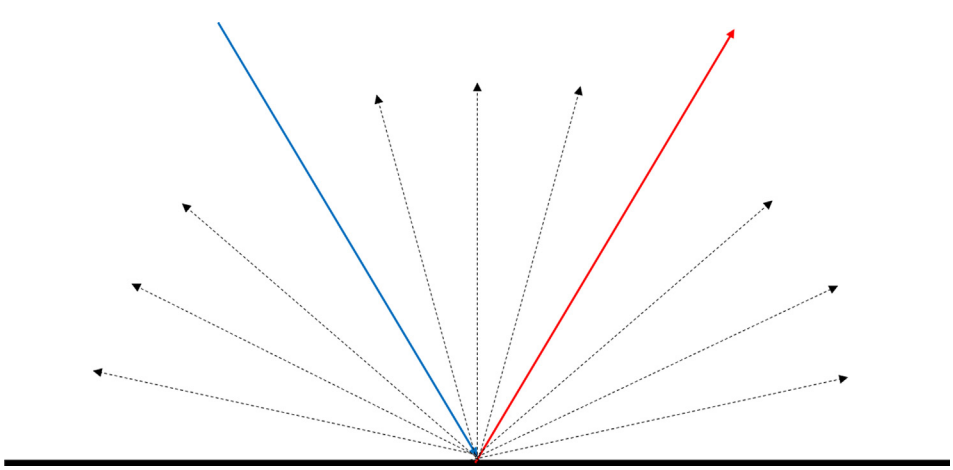

Fig. 1. The conceptual model of gas molecular reflection on the rough surface (wall) of porous media. The solid arrow line represents the specular reflection, while the dash arrow lines represent the diffusive reflection.

2.3. Kinetic theory of gasses and viscosity of gas mixtures

In the bulk flow, consider a spherical coordinate system in which a small volume $d\tau$ of the gas is in a position (r, φ, ω), as shown in Fig. 2. According to the kinetic theory of gasses [3], in unit time the number of the ith type of molecules that collide once in $d\tau$, then leave $d\tau$ and reach a small area dS at (0,0,0) without any other collisions is

$$dN_i = x_i \frac{\bar{v}_i n_t \cdot d\tau}{\lambda_i} \frac{\cos\varphi}{4\pi r^2} \exp\left(-\frac{r}{\lambda_i}\right) \cdot dS \tag{7}$$

In the above formulation, $x_i$is the mole concentration of component i. n is the number density of the gas mixture. r is the traveling distance.

The average momentum the molecules transport can be calculated by multiplying their flux velocity (in the mean moving distance controlled by mean free path) by their number density and mass.

For laminar flow (along x-direction as shown in Fig. 3), suppose there is no wall and no boundary reflection, then given an imaginary plain at $z = z_0$with unit area in the space, molecules that impinge into the unit area from position (r, φ, ω) have the flux velocity at $z = z_0 + r\cos\varphi$, as shown in Fig. 4. In this sense, assuming simple mixing rule, the amount of horizontal momentum transported by ith type of molecules impinge into the imaginary plain from above is

$$M_{ui} = x_i \frac{\bar{v}_i m_i n}{4\pi\lambda_i} \int_0^{2\pi}\int_0^{\pi/2}\int_0^{\infty} u(z_0 + r\cos\varphi)\cos\varphi\sin\varphi \exp\left(-\frac{r}{\lambda_i}\right) dr d\varphi d\omega \tag{8}$$

where u is the flux velocity. In the case of laminar flow, u is the function of z only. Since the space is open, the traveling distance of the molecular may range from 0 to infinity. Therefore, the lower and upper limit of the inner integral is 0 and ∞ respectively. (This will be different for rarefied gases within microchannels).

Similarly, the horizontal momentum carried by ith of molecules from bottom along direction (π-φ) is

$$M_{bi} = x_i \frac{\bar{v}_i m_i n}{4\pi\lambda_i} \int_0^{2\pi}\int_0^{\pi/2}\int_0^{\infty} u(z_0 - r\cos\varphi)\cos\varphi\sin\varphi \exp\left(-\frac{r}{\lambda_i}\right) dr d\varphi d\omega \tag{9}$$

Then, by summing up all N_C types of molecules, the total momentum from above direction and bellow direction can be calculated and expanded into second-order in (10) and (11), respectively.

$$\begin{aligned} M_u &= \sum_{i=1}^{N_C} M_{ui} = \sum_{i=1}^{N_C} x_i \frac{\bar{v}_i m_i n}{4\pi\lambda_i} \int_0^{2\pi}\int_0^{\pi/2}\int_0^{\infty} u(z_0 + r\cos\varphi)\cos\varphi\sin\varphi \exp\left(-\frac{r}{\lambda_i}\right) dr d\varphi d\omega \\ &= \sum_{i=1}^{N_C} x_i \frac{\bar{v}_i m_i n}{4\pi\lambda_i} \int_0^{2\pi}\int_0^{\pi/2}\int_0^{\infty} \left[u|_{z_0} + r\cos\varphi\left(\frac{\partial u}{\partial z}\right)\Big|_{z_0} + \frac{1}{2} r^2 \cos^2\varphi \left(\frac{\partial^2 u}{\partial z^2}\right)\Big|_{z_0} \right] \cos\varphi\sin\varphi \exp\left(-\frac{r}{\lambda_i}\right) dr d\varphi d\omega \end{aligned} \tag{10}$$

$$\begin{aligned} M_b &= \sum_{i=1}^{N_C} M_{bi} = \sum_{i=1}^{N_C} x_i \frac{\bar{v}_i m_i n}{4\pi\lambda_i} \int_0^{2\pi}\int_0^{\pi/2}\int_0^{\infty} u(z_0 - r\cos\varphi)\cos\varphi\sin\varphi \exp\left(-\frac{r}{\lambda_i}\right) dr d\varphi d\omega \\ &= \sum_{i=1}^{N_C} x_i \frac{\bar{v}_i m_i n_i}{4\pi\lambda_i} \int_0^{2\pi}\int_0^{\pi/2}\int_0^{\infty} \left[u|_{z_0} - r\cos\varphi\left(\frac{\partial u}{\partial z}\right)\Big|_{z_0} + \frac{1}{2} r^2 \cos^2\varphi \left(\frac{\partial^2 u}{\partial z^2}\right)\Big|_{z_0} \right] \cos\varphi\sin\varphi \exp\left(-\frac{r}{\lambda_i}\right) dr d\varphi d\omega \end{aligned} \tag{11}$$

The shear force on the plain is just the difference between M_u and M_b as

$$\tau = M_u - M_b = \frac{1}{3} \sum_{i=1}^{N_C} x_i \bar{v}_i m_i n \lambda_i \left(\frac{\partial u}{\partial z}\right)\Big|_{z_0} \tag{12}$$

Based on the definition of viscosity, we can obtain the viscosity of gas mixture as

$$\mu_{ideal} = \frac{1}{3} \sum_{i=1}^{N_C} x_i \bar{v}_i m_i n \lambda_i \tag{13}$$

According to [3], the accuracy of the above approach is up to 90% for light molecules. In this sense, we can use this mean free path method originated from the kinetic theory of gases to estimate the viscosity of ideal gas mixtures.

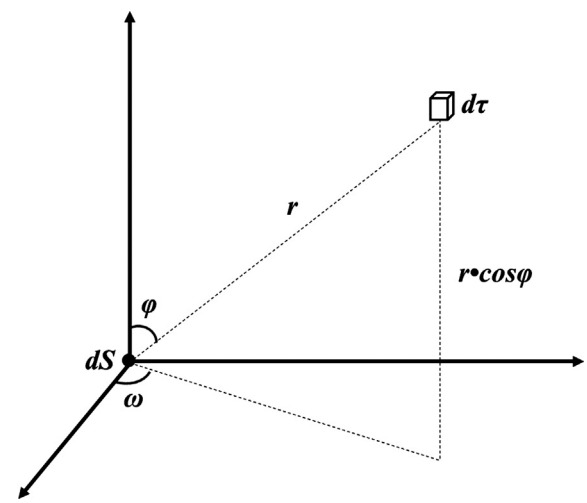

Fig. 2. Coordinate system showing the relative position of dS and $d\tau$.

In a system that is confined by walls, gas molecules cannot travel freely as they do in the open-boundary flow. The molecules will frequently collide with the walls losing momentum, which causes the reduction of viscous shear stress and the slippage of the flow. Based on this model, we can further calculate the slippage boundary condition of gas mixtures by putting the mixture into a confined flow channel.

3. Non-empirical slippage model

In this section, we present the derivation of our non-empirical gas slippage model of gas mixtures.

As mentioned in the previous sections, the existence of walls and diffusive reflection is the origin of viscosity reduction as well as boundary slippage. We consider two types of molecules. For the first type, these molecules have a molecular collision at (r, φ, ω), then directly impinge on a point of interest (of unit area) on the boundary ($z = 0$) along direction φ, as shown in Fig. 5.

According to our previous discussion, the flux velocity transported by these molecules is the flux velocity at $z = r\cdot\cos\varphi$. Because of the confinement of the upper wall, the traveling distance of Type 1 molecules ranges from 0 to $d/\cos\varphi$. All the effective momentum transported by all types of molecules can be calculated as

$$M_1 = \sum_{i=1}^{N_C} M_{1i} = \sum_{i=1}^{N_C} x_i \frac{\bar{v}_i m_i n}{4\pi} \int_0^{2\pi}\int_0^{\pi/2}\int_0^{d/\cos\varphi} u(r\cos\varphi)\cos\varphi\sin\varphi dr \exp\left(-\frac{r}{\lambda_i}\right) dr d\varphi d\omega \tag{14}$$

The above formulation can be expanded to the second order as

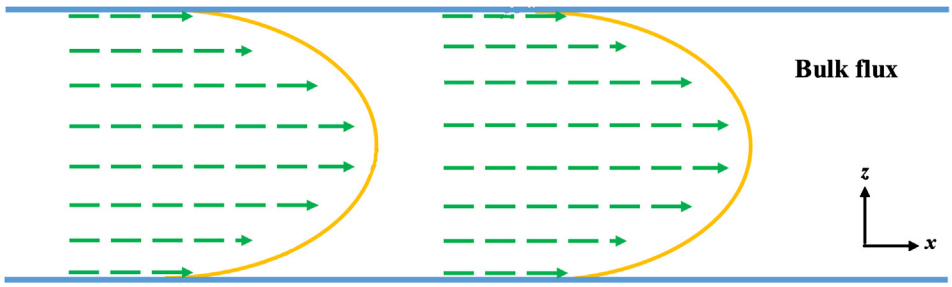

Fig. 3. The velocity profile of the laminar flow system.

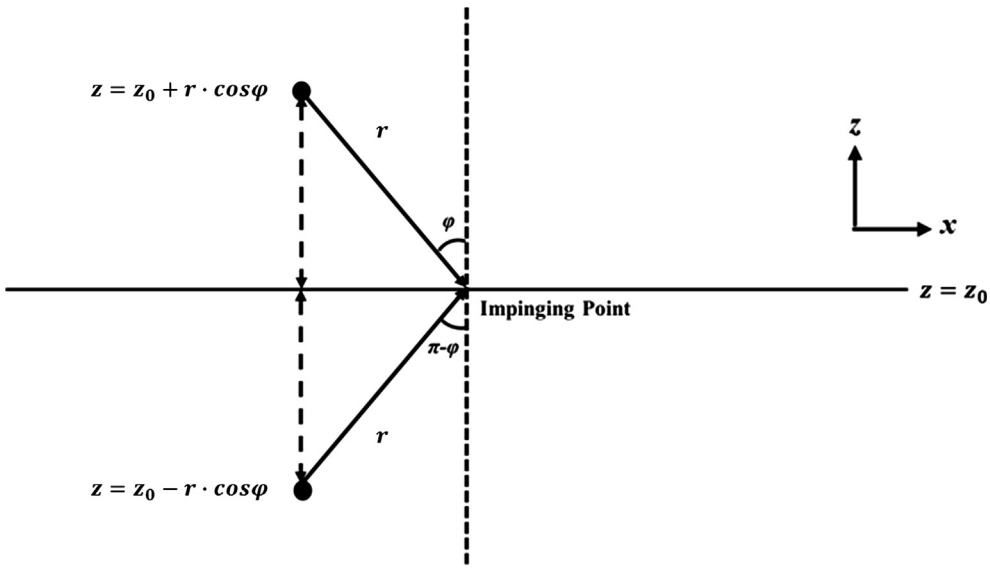

Fig. 4. The conceptual model of the *i*th type of molecules that impinge into an imaginary plain in an open space within a laminar flow field. *x*-direction is the flux direction, meaning that the flux velocity vector only has non-zero components along the *x*-direction.

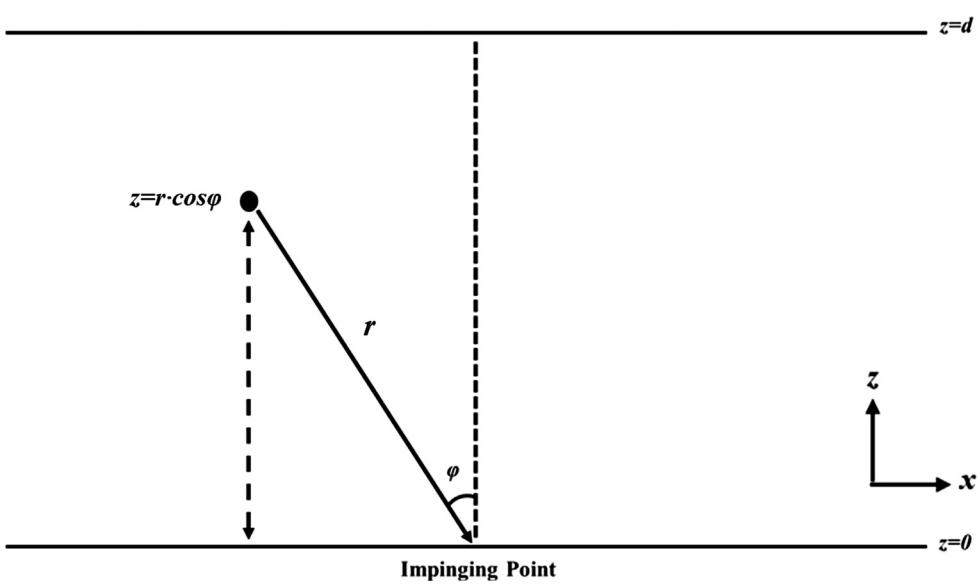

Fig. 5. The conceptual model of Type 1 molecules.

$$M_1 = \sum_{i=1}^{N_C} M_{1i} \approx \sum_{i=1}^{N_C} x_i \frac{\bar{v}_i m_i n}{4\pi} \int_0^{2\pi}\int_0^{\pi/2}\int_0^{d/\cos\varphi} \left[u|_w + r\cos\varphi\left(\frac{\partial u}{\partial z}\right)\Big|_w + \frac{1}{2} r^2 \cos^2\varphi \left(\frac{\partial^2 u}{\partial z^2}\right)\Big|_w \right] \cos\varphi \sin\varphi \exp\left(-\frac{r}{\lambda_i}\right) dr d\varphi d\omega \tag{15}$$

$$\sigma(M_1 + W_2) = \sum_{i=1}^{N_C} x_i \frac{\bar{v}_i m_i n}{3} \lambda_i \left(\frac{\partial u}{\partial z}\right)\Big|_w \tag{20}$$

By reorganizing the above equation and considering $\bar{v}_i \propto (\sqrt{m_i})^{-1}$, the slippage boundary condition can be obtained as

$$u|_w = \frac{2\sum_{i=1}^{N_C} x_i\sqrt{m_i}\lambda_i \begin{Bmatrix} 2-\sigma-\sigma(1-\sigma)\exp(-2K_{Ni}^{-1})[4K_{Ni}^{-3}+2K_{Ni}^{-2}-K_{Ni}^{-1}+1]+\sigma(1-2\sigma)K_{Ni}^{-3}Ei(-K_{Ni}^{-1}) \\ +\sigma\exp(-K_{Ni}^{-1})[(1-2\sigma)K_{Ni}^{-2}-(1-2\sigma)K_{Ni}^{-1}+(2-\sigma)] \end{Bmatrix}}{3\sigma\sum_{i=1}^{N_C} x_i\sqrt{m_i}\begin{Bmatrix} 1+\sigma K_{Ni}^{-2}Ei(-K_{Ni}^{-1})+\sigma\exp(-K_{Ni}^{-1})[K_{Ni}^{-1}-1] \\ +4(1-\sigma)K_{Ni}^{-2}Ei(-2K_{Ni}^{-1})+(1-\sigma)\exp(-2K_{Ni}^{-1})[2K_{Ni}^{-1}-1] \end{Bmatrix}\sum_{j=1}^{Nc} x_j\lambda_j} \lambda_{fm}\left(\frac{\partial u}{\partial z}\right)\Big|_w - \frac{\sum_{i=1}^{N_C} x_i\sqrt{m_i}\lambda_i^2 \begin{Bmatrix} 6+(-8+11\sigma)K_{Ni}^{-4}Ei(-K_{Ni}^{-1})+16(1-\sigma)K_{Ni}^{-4}Ei(-2K_{Ni}^{-1}) \\ -(1-\sigma)\exp(-2K_N^{-1})[-8K_{Ni}^{-3}+4K_{Ni}^{-2}-4K_{Ni}^{-1}+6] \\ +\exp(-K_{Ni}^{-1})[(-8+11\sigma)K_{Ni}^{-3}+(8-11\sigma)K_{Ni}^{-2}+(-16+10\sigma)K_{Ni}^{-1}-6\sigma] \end{Bmatrix}}{12\sum_{i=1}^{N_C} x_i\sqrt{m_i}\begin{Bmatrix} 1+\sigma K_{Ni}^{-2}Ei(-K_{Ni}^{-1})+\sigma\exp(-K_{Ni}^{-1})[K_{Ni}^{-1}-1] \\ +4(1-\sigma)K_{Ni}^{-2}Ei(-2K_{Ni}^{-1})+(1-\sigma)\exp(-2K_{Ni}^{-1})[2K_{Ni}^{-1}-1] \end{Bmatrix}\left(\sum_{j=1}^{Nc} x_j\lambda_j\right)^2} \lambda_{fm}^2\left(\frac{\partial^2 u}{\partial z^2}\right)\Big|_w \tag{21}$$

Eq. (15) can be calculated analytically as

$$\begin{aligned} M_1 = &\sum_{i=1}^{N_C} x_i \frac{\bar{v}_i m_i n}{48}\lambda_i^2\left(\frac{\partial^2 u}{\partial z^2}\right)\Big|_w \{6 + 3K_{Ni}^{-4}Ei(-K_{Ni}^{-1}) \\ &-\exp(-K_{Ni}^{-1})[-3K_{Ni}^{-3}+3K_{Ni}^{-2}+6K_{Ni}^{-1}+6]\} \\ \ldots &+ \sum_{i=1}^{N_C} x_i \frac{\bar{v}_i m_i n}{48}\lambda_i\left(\frac{\partial u}{\partial z}\right)\Big|_w \{8 + 8K_{Ni}^{-3}Ei(-K_{Ni}^{-1}) + \exp(-K_{Ni}^{-1})[8K_{Ni}^{-2}-8K_{Ni}^{-1}-8]\} \\ \ldots &+ \sum_{i=1}^{N_C} x_i \frac{\bar{v}_i m_i n}{48} u|_w \{12 + 12K_{Ni}^{-2}Ei(-K_{Ni}^{-1}) + \exp(-K_{Ni}^{-1})[12K_{Ni}^{-1}-12]\} \end{aligned} \tag{16}$$

Another type of molecules hit the upper wall before impinging, as shown in Fig. 6. Because of the confinement of the upper wall, Type 2 molecules have momentum loss at the upper wall. The traveling distance of Type 2 molecules range from $d/\cos\varphi$ to $2d/\cos\varphi$. Consider the symmetric feature of specular reflection, the z coordinate of Type 2 molecules whose traveling distance is r is $2d-r\cdot\cos\varphi$.

The effective momentum transported by Type 2 molecules is shown in (17). Similarly to the treatment of Type 1 molecules, Eq. (17) can be expanded to the second order, as shown in Eq. (18).

$$M_2 = (1-\sigma)\sum_{i=1}^{N_C} x_i \frac{\bar{v}_i m_i n}{4\pi\lambda_i}\int_0^{2\pi}\int_0^{\pi/2}\int_{d/\cos\varphi}^{2d/\cos\varphi} u(2d-r\cos\varphi)\cos\varphi\sin\varphi\exp\left(-\frac{r}{\lambda_i}\right) dr d\varphi d\omega \tag{17}$$

$$M_2 \approx (1-\sigma)\sum_{i=1}^{N_C} x_i \frac{\bar{v}_i m_i n}{4\pi\lambda_i}\int_0^{2\pi}\int_0^{\pi/2}\int_{d/\cos\varphi}^{2d/\cos\varphi} \begin{bmatrix} u|_w + (2d-r\cos\varphi)\left(\frac{\partial u}{\partial z}\right)\Big|_w \\ + \frac{1}{2}(2d-r\cos\varphi)^2\left(\frac{\partial^2 u}{\partial z^2}\right)\Big|_w \end{bmatrix} \cos\varphi\sin\varphi\exp\left(-\frac{r}{\lambda_i}\right) dr d\varphi d\omega \tag{18}$$

The above formulation can be evaluated analytically as

$$\begin{aligned} M_2 = (1-\sigma)&\sum_{i=1}^{N_C} x_i \frac{\bar{v}_i m_i n}{48}\lambda_i^2\left(\frac{\partial^2 u}{\partial z^2}\right)\Big|_w \begin{Bmatrix} -11K_{Ni}^{-4}Ei(-K_{Ni}^{-1}) + \exp(-K_{Ni}^{-1})[-11K_{Ni}^{-3}+11K_{Ni}^{-2}-10K_{Ni}^{-1}+6] \\ +16K_{Ni}^{-4}Ei(-2K_{Ni}^{-1})-\exp(-2K_N^{-1})[-8K_{Ni}^{-3}+4K_{Ni}^{-2}-4K_{Ni}^{-1}+6] \end{Bmatrix} \\ \ldots &+ (1-\sigma)\sum_{i=1}^{N_C} x_i \frac{\bar{v}_i m_i n}{48}\lambda_i\left(\frac{\partial u}{\partial z}\right)\Big|_w \begin{Bmatrix} -16K_{Ni}^{-3}Ei(-K_{Ni}^{-1})-\exp(-K_{Ni}^{-1})[16K_{Ni}^{-2}-16K_{Ni}^{-1}+8] \\ +32K_{Ni}^{-3}Ei(-2K_{Ni}^{-1}) + \exp(-2K_{Ni}^{-1})[16K_{Ni}^{-2}-8K_{Ni}^{-1}+8] \end{Bmatrix} \\ \ldots &+ (1-\sigma)\sum_{i=1}^{N_C} x_i \frac{\bar{v}_i m_i n}{48} u|_w \begin{Bmatrix} -12K_{Ni}^{-2}Ei(-K_{Ni}^{-1}) + \exp(-K_{Ni}^{-1})[-12K_{Ni}^{-1}+12] \\ +48K_{Ni}^{-2}Ei(-2K_{Ni}^{-1}) + \exp(-2K_{Ni}^{-1})[24K_{Ni}^{-1}-12] \end{Bmatrix} \end{aligned} \tag{19}$$

The summation of Eq. (16) and Eq. (19) is the actual horizontal momentum transferred to the wall. By equating the actual horizontal momentum with the ideal horizontal momentum as shown in Equation (12) and considering the loss of momentum at the impinging point, we can obtain the 'equivalent' slippage velocity that generates the apparent mass flow rate, as shown in

Compared with Eq. (2), the two coefficients C_1 and C_2 in our model are as follows

$$C_1 = \frac{2\sum_{i=1}^{N_C} x_i\sqrt{m_i}\lambda_i \begin{Bmatrix} 2-\sigma-\sigma(1-\sigma)\exp(-2K_{Ni}^{-1})[4K_{Ni}^{-3}+2K_{Ni}^{-2}-K_{Ni}^{-1}+1] \\ +\sigma(1-2\sigma)K_{Ni}^{-3}Ei(-K_{Ni}^{-1}) \\ +\sigma\exp(-K_{Ni}^{-1})[(1-2\sigma)K_{Ni}^{-2}-(1-2\sigma)K_{Ni}^{-1}+(2-\sigma)] \end{Bmatrix}}{3\sigma\sum_{i=1}^{N_C} x_i\sqrt{m_i}\begin{Bmatrix} 1+\sigma K_{Ni}^{-2}Ei(-K_{Ni}^{-1})+\sigma\exp(-K_{Ni}^{-1})[K_{Ni}^{-1}-1] \\ +4(1-\sigma)K_{Ni}^{-2}Ei(-2K_{Ni}^{-1})+(1-\sigma)\exp(-2K_{Ni}^{-1})[2K_{Ni}^{-1}-1] \end{Bmatrix}\sum_{j=1}^{Nc} x_j\lambda_j} \tag{22}$$

$$C_2 = \frac{\sum_{i=1}^{N_C} x_i\sqrt{m_i}\lambda_i^2 \begin{Bmatrix} 6+(-8+11\sigma)K_{Ni}^{-4}Ei(-K_{Ni}^{-1})+16(1-\sigma)K_{Ni}^{-4}Ei(-2K_{Ni}^{-1}) \\ -(1-\sigma)\exp(-2K_N^{-1})[-8K_{Ni}^{-3}+4K_{Ni}^{-2}-4K_{Ni}^{-1}+6] \\ +\exp(-K_{Ni}^{-1})[(-8+11\sigma)K_{Ni}^{-3}+(8-11\sigma)K_{Ni}^{-2}+(-16+10\sigma)K_{Ni}^{-1}-6\sigma] \end{Bmatrix}}{12\sum_{i=1}^{N_C} x_i\sqrt{m_i}\begin{Bmatrix} 1+\sigma K_{Ni}^{-2}Ei(-K_{Ni}^{-1})+\sigma\exp(-K_{Ni}^{-1})[K_{Ni}^{-1}-1] \\ +4(1-\sigma)K_{Ni}^{-2}Ei(-2K_{Ni}^{-1})+(1-\sigma)\exp(-2K_{Ni}^{-1})[2K_{Ni}^{-1}-1] \end{Bmatrix}\left(\sum_{j=1}^{Nc} x_j\lambda_j\right)^2} \tag{23}$$

4. Results and discussion

4.1. Validation

In this section, we validate our proposed model using data in literature. We compare our model with the work of Bentz et al [79], Sharipov et al. [74], Hyakutake et al. [77] and Yamaguchi el al. [80].

Bentz et al. measure the mass transfer of rarefied gas mixtures using spinning rotor gauge. Sharipov et al. calculate the mass transfer of several combinations of binary gas mixtures by solving linearized Boltzmann equation. To quantify the interaction between different gas molecules, Sharipov et al. consider both hard sphere gas molecules and Lennard-Johns potential. The results between the two models are

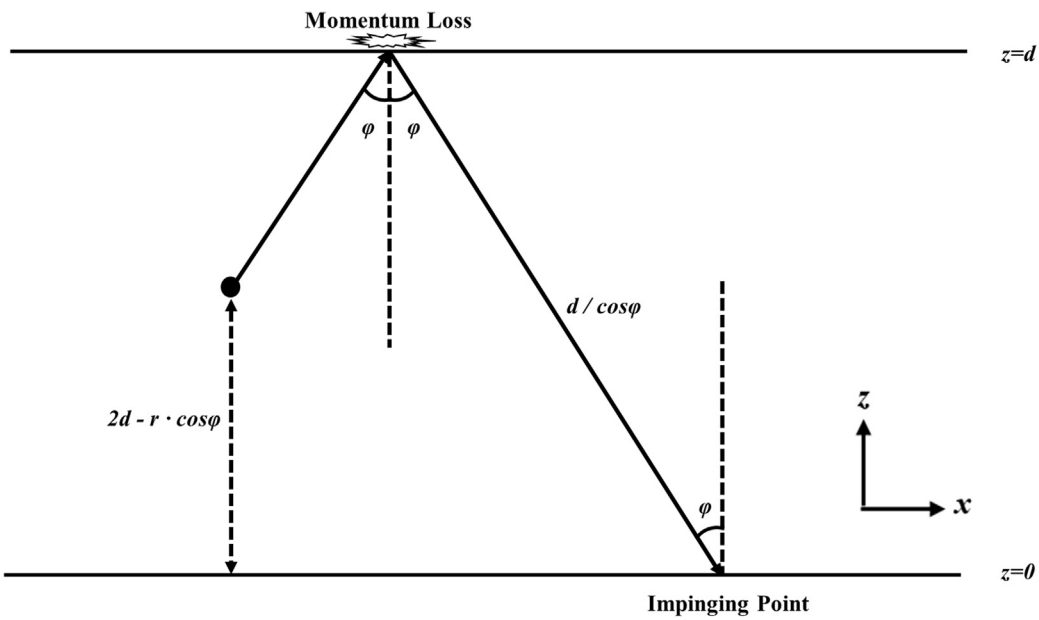

Fig. 6. The conceptual model of Type 2 molecules.

slightly different. Hyakutake et al. conduct combine molecular dynamics (MD) simulation with DSMC to simulate the transport of binary gas mixtures in micro-channels. Yamaguchi el al. conduct microtube flooding to measure the slippage coefficient of binary gas mixtures. The above works has been widely adopted as benchmarks in the study of the rarefied gas flow of multicomponent gases.

4.1.1. Single component case

We first use Li et al. [31]'s and Shen et al. [85]'s numerical results to as benchmark data to validate our results for the single-component case. Li et al. used Lattice Boltzmann Method (LBM) with combined bounce-back/specular-reflection boundary to simulate gas transport in microchannels. In both of the two referred work, purely diffusive reflection on the boundary is assumed (TMAC = 1). In this paper, we compared the dimensionless flow rate Q_D predicted by the slippage models. The dimensionless flow rate is defined as follows

$$Q_D = -\int_0^h \rho u dz \sqrt{2RT}/(h^2 \partial p/\partial x) \tag{24}$$

For our proposed correlation, Q_D can be explicitly expressed as

$$Q_D = \frac{\sqrt{\pi}}{12K_N} + \frac{\sqrt{\pi}}{2}C_1 + \sqrt{\pi}K_N C_2 \tag{25}$$

When reduced to single component cases, our kinetic model is independent of molecular type. However, Yamaguchi et al. [80] and Bentz et al. [79]'s model are slightly impacted by the type of components. Regarding this, we compare the mass transfer rate predicted by the above two models with both Helium (He) and Argon (Ar).

The comparison of mass transfer is shown in Fig. 7, from which it can be seen that our proposed model matches numerical experimental results very well. Especially, when Knudsen number is above 0.5, our model yields more accurate results than the other four models. This is partly attributed to the second-order correction term in our correlation.

We also compare our results with Maurer et al. [86]'s experimental data. The experiment is based on microchannel flooding using Helium with Knudsen number up to 0.8. The TMAC was determined as 0.91 ± 0.03. The microchannel used for the flow rate measurement was shallow enough so that the flow channel can be viewed as two infinite long parallel plates. Maurer et al.'s experiment has been widely adopted as benchmark data for the validation of gas slippage models. In this work, we compare the flow rate enhancement factor predicted by our model with that predicted by Maurer et al.'s experiment. The flow rate enhancement factor, as defined in [62], can be calculated analytically by our model, as shown in the equation below.

$$S = 1 + 6C_1K_N + 12C_2K_N^2 \tag{26}$$

In the above equation, C_1 and C_2 is as defined in Eqs. (22) and (23) respectively. The comparison with Knudsen number up to 0.8 is shown in Fig. 8, from which it can be seen that our model is with 90% accuracy.

4.1.2. Multiple component cases

In this section, we validate our model for multiple component (binary gas mixtures) cases. We use the binary mixture of Helium-Argon (He-Ar) and Helium-Xenon (He-Xe). The collision diameter of Helium, Argon and Xenon is 260 pm, 341 pm and 398 pm respectively [87]. Diffusive reflection (TMAC = 1) is used for the validation. The comparison of the dimensionless flow rate for binary He-Ar gas mixture and binary He-Xe gas mixture with different mole fraction of He is shown in Fig. 8 and Fig. 9 respectively. (The work of Yamaguchi et al. [80] and Bentz et al. [79] only has data for He-Ar mixtures.)

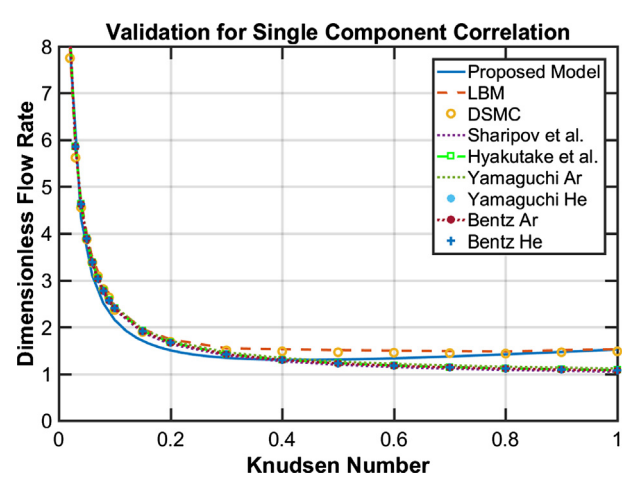

Fig. 7. Comparison between LBM results, DSMC results, physical experimental data and the proposed kinetic model for single component gas flow with TMAC being 1.

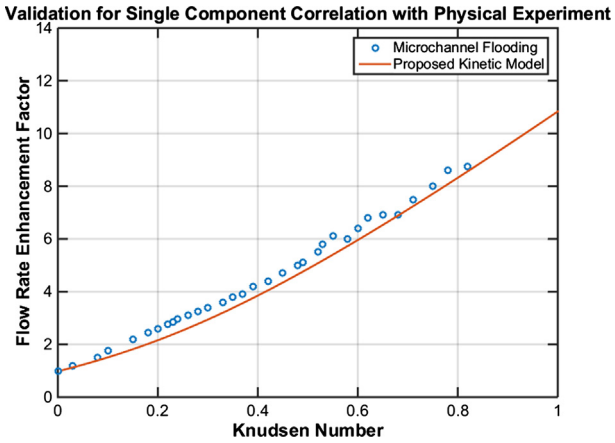

Fig. 8. Comparison of flow rate enhancement factor between our model and Maurer et al.'s microchannel flooding experiment with TMAC being 0.91.

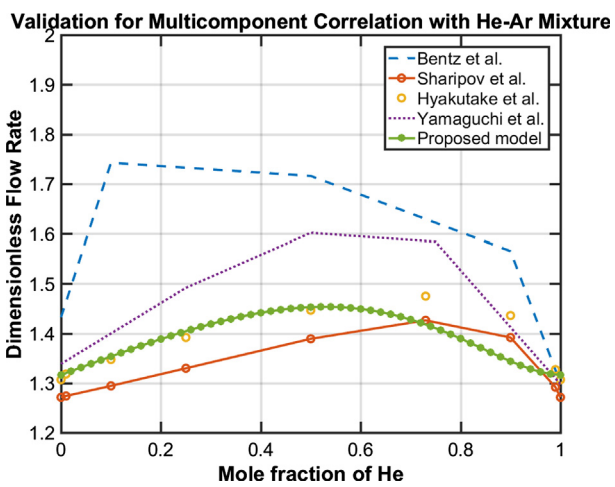

Fig. 9. Comparison of the dimensionless flow rate for binary He-Ar gas mixture with varying mole fraction of He.

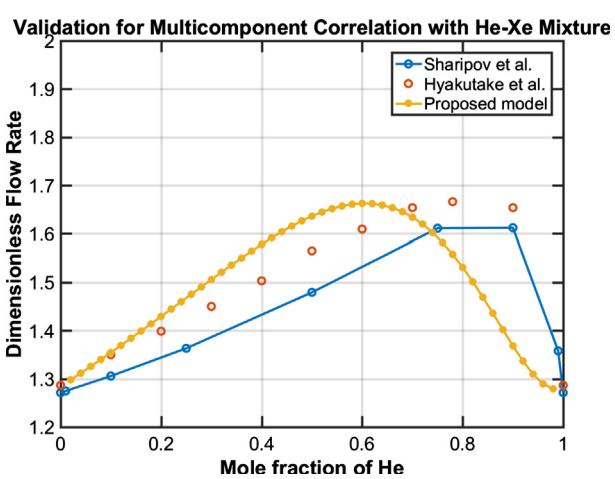

Fig. 10. Comparison of the dimensionless flow rate for binary He-Xe gas mixture with varying mole fraction of He.

As shown in Fig. 9 and Fig. 10, our model predicts the same trend with literature data. The average difference between our model with literature data is less than 10%. The Knudsen number used for this calculation is 0.4. When Knudsen number varies within the range from 0 to 1, the difference between our model with literature data varies from 0.9% ($K_N < 0.01$) to 12% ($K_N = 0.18$).

Table 1
Summary of concentration combinations of nitrogen-oxygen mixture cases.

	Nitrogen	Oxygen
Case 1 (100 nm)	78%	22%
Case 2 (100 nm)	100%	0%
Case 3 (100 nm)	0%	100%

The maximum value of the mass transfer rate is at $x_{He} = 0.6 \sim 0.8$. This is because heavier components have larger impact on the slippage than lighter components.

It should be mentioned that in Hyakutake et al.'s work, TMAC is not 1. Instead, the TMAC (at T = 300 K) of Ar and Xe is respectively 0.89 and 0.95. In our work, we assume the TMAC of all components are the same. Such assumption can be easily relaxed in the future work. Typically, smaller TMAC leads higher mass transfer rate. If we substitute the TMAC used in Hyakutake et al.'s work, the mass transfer rate predicted by our model will increase by less than 5%.

4.2. Results

In this section, we present the flow rate enhancement factor S of a binary and ternary gas mixtures predicted by our proposed correlation. The properties of gases used in this work are all from widely cited literature [88].

4.2.1. Slippage of air (a binary mixture of nitrogen-oxygen)

In this section, we present the impact of compositional distribution on the flow rate enhancement factor, shown in Eq. (26), of binary mixtures of nitrogen and oxygen, which is a mimic of air. The summary of the concentration combinations is listed in Table 1. The pressure ranges from 0.4 bar to 10 bar. The width of the flow channel is 100 nm. The flow rate enhancement factor is show in Fig. 11.

As pressure increases, flow rate enhancement factor decreases from above 20 to 1.

4.2.2. Slippage of a binary mixture of hydrogen-oxygen

In this section, we present the impact of compositional distribution on the flow rate enhancement factor of binary mixtures of hydrogen and oxygen. The study of hydrogen-oxygen mixtures is crucial to the determination of explosion limit in micro devices [89].

We compare the flow rate enhancement factor of the binary mixture with that of pure components. The summary of the concentration combinations is listed in Table 2.

The flow rate enhancement factors of three cases are shown in Fig. 12. From Fig. 12 it can be seen that gases with smaller molecular weight have higher slippage effect. On the other hand, in a mixture, the slippage effect prone to the component with higher molecular weight.

4.2.3. Ternary mixtures of light hydrocarbon

In this sub-section, we discuss the impact of compositional distribution on the ternary mixture of light hydrocarbons. For hydrocarbons in unconventional gas reservoirs, the flow rate enhancement factor is also known as the permeability enhancement factor. In this work, we calculate the permeability enhancement factor of a ternary mixture of methane (C1), ethane (C2) and propane (C3). The summary of the compositional combinations is listed in Table 3. The permeability enhancement factor with respect to pressure for the 25 nm wide channel and the 15 nm wide channel is shown in Fig. 13 and Fig. 14, respectively. From the two figures, we can see that when pressure is above 2000 psi, the permeability enhancement factor is below 2. This indicates that Klinkenberg effect is more important in the near-well region of a reservoir and also in the late-production regime during production. As can be seen from the results, our proposed correlation is able to capture the compositional impact for ternary gas mixtures.

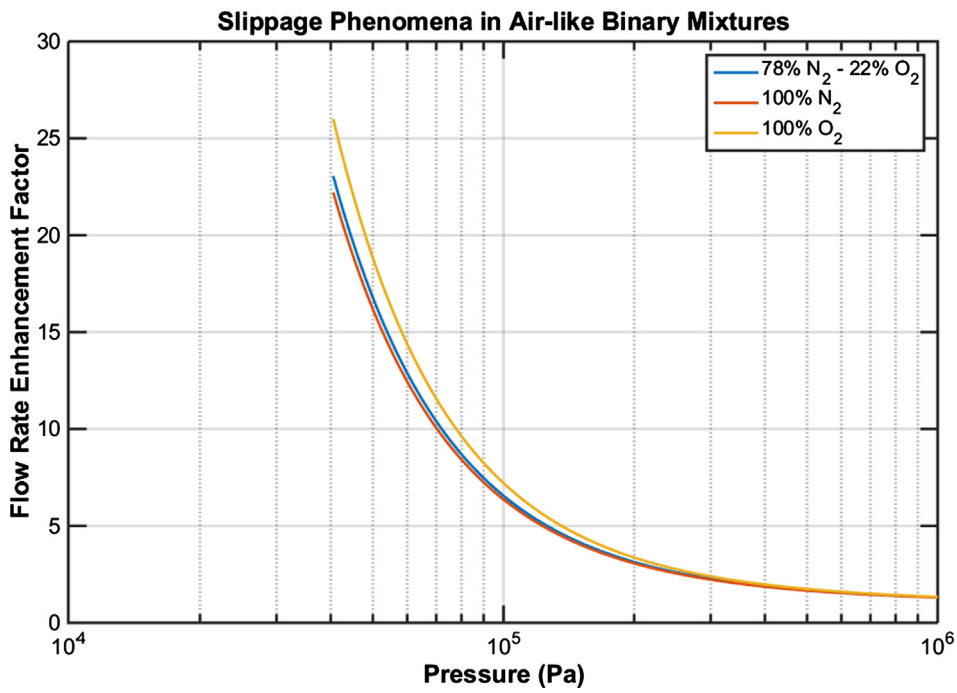

Fig. 11. Flow rate enhancement of air-like binary mixtures of nitrogen and oxygen within a 100 nm microchannel.

Table 2
Summary of concentration combinations of hydrogen-oxygen mixture cases.

	Hydrogen	Oxygen
Case 4 (100 nm)	50%	50%
Case 5 (100 nm)	100%	0%
Case 6 (100 nm)	0%	100%

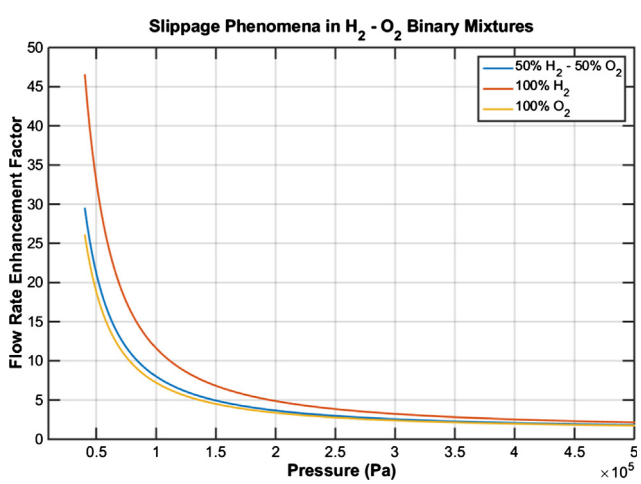

Fig. 12. Flow rate enhancement of hydrogen-oxygen binary mixtures within a 100 nm microchannel.

Table 3
Summary of concentration combinations of ternary mixture cases.

	Methane	Ethane	Propane
Case 7 (25 nm)	10%	20%	70%
Case 8 (25 nm)	33.3%	33.3%	33.3%
Case 9 (25 nm)	70%	20%	10%
Case 10 (15 nm)	10%	20%	70%
Case 11 (15 nm)	33.3%	33.3%	33.3%
Case 12 (15 nm)	70%	20%	10%

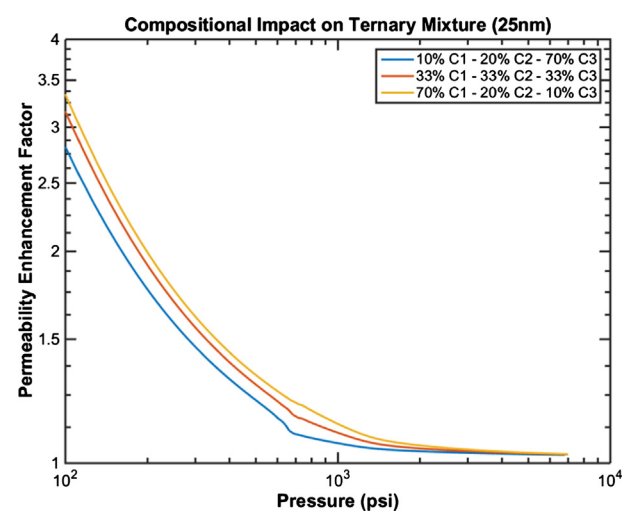

Fig. 13. Permeability enhancement factor for different composition distribution of methane-ethane-propane mixtures within 25 nm channel with respect to pressure. Both of the two axes are in log scale.

Moreover, there should be not much difficulty for our correlation to predict the permeability enhancement effect of more complex gas mixtures consisting of light components.

4.3. Discussion

As can be seen from the validation and resutls, our model can accurately capture the multicomponent sippage effect with finite Knudsen numbers up to 1. For higher Knudsen numbers, our model may show larger errors because the gas-wall interaction becomes more complex. In higher Knudsen number conditions (transient regime), the molecules collide with the wall more frequently, and the behavior of the gases can no more be described by viscosity-shear force relationship. For that condition, more 'discrete' models need to be adopted. Moreover, we now consider two types of molecules. As Knudsen number becomes larger, more molecules will hit the wall more than once before

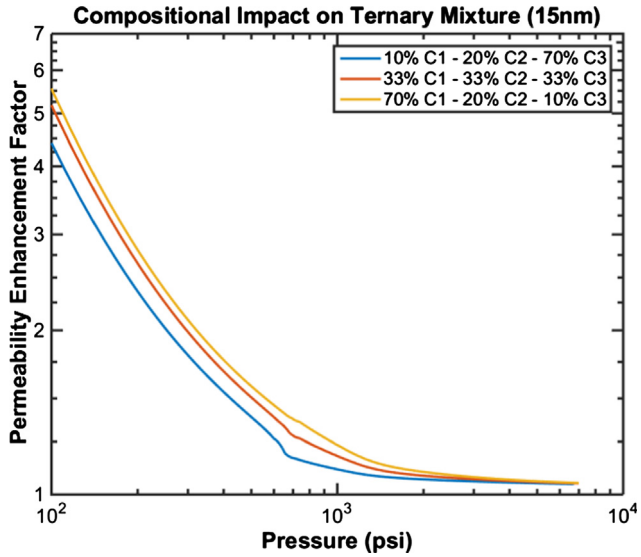

Fig. 14. Permeability enhancement factor for different composition distribution of methane-ethane-propane mixtures within 15 nm channel with respect to pressure. Both of the two axes are in log scale.

impinging into the point of interest. Hence the contribution of these currently-ignored molecules will become larger, especially when TMAC is not 1.

Admittedly, our model has several limitations. First, it can only be used to low-speed gas flow, because it assumes near-steady conditions in its derivation. Secondly, it should only be applied to light gas component in near-ideal (low pressure) conditions, since it is based on the assumption of hard-sphere gas collisions among different gas specifies. For high-pressure condition, as pointed on by Long et al. [90], the confinement effect cannot be ignored and our model cannot handle this condition. For heavier components, the molecular-molecular interaction becomes more complex and the hard-sphere collision assumption is no more validate. Lennard-Jones potential should be taken into consideration [24]. Thirdly, it does not take account for the surface force impact [91], surface shape impact [46] and dense gas effect [52]. The model can be further improved by considering the variation of gas density near the boundary. Without the incorporation of multiphase slippage effect [92,93], The applications of the model should be limited to single phase flow for the time being.

In real practice, our model could either be combined with digital rock techniques [56] for small scale simulation or be directly used as a gas apparent permeability correlation in reservoir scale simulation. In the former case, our model provides the boundary condition for the governing equations (Navier-Stokes equation, Burnett equation, etc.). In the latter case, our model serves as a Klinkenberg-type correlation, as shown in Equation (26), for the calculation of gas apparent permeability. Since the model is non-empirical, it only requires the effective rock diameter, TMAC and gas component concentration as the input parameters, making it convenient for real applications.

5. Summary and conclusion

To sum up, in this work, we have derived a novel non-empirical model to quantify the gas slippage effect for multicomponent gas mixtures. Based on the kinetic theory of gases, our model has a solid physical foundation. It has been validated against molecular simulation results and has shown good accuracy for low to moderate Knudsen numbers ($K_N < 1$).

To the best our knowledge, this work is among the first non-empirical gas-slippage correlations for gas mixtures. It is promising that the proposed model will be applied to the design of MEMS device [14] and reservoir simulation of unconventional gas formations [94].

Acknowledgment

This work was supported by CNPC-USA and Energi Simulation.

References

[1] Maxwell C. On stresses in rarified gases arising from inequalities of temperature on JSTOR. Philos Trans R Soc London 1879;170:231–56. https://doi.org/10.1098/rstl.1879.006.
[2] Hadjiconstantinou NG. The limits of Navier-Stokes theory and kinetic extensions for describing small-scale gaseous hydrodynamics. Phys Fluids 2006;18:111301https://doi.org/10.1063/1.2393436.
[3] Present RD. Kinetic theory of gases. McGraw-Hill; 1958.
[4] Chapman S, Cowling TG, Thomas G. The mathematical theory of non-uniform gases; an account of the kinetic theory of viscosity, thermal conduction and diffusion in gases. Cambridge University Press; 1970.
[5] Cercignani C. The Boltzmann equation and its applications. New York, NY: Springer, New York, NY; 1988. doi: 10.1007/978-1-4612-1039-9_2.
[6] Knudsen M. Thermischer Molekulardruck der Gase in Röhren und porösen Körpern. Ann Phys 1910;336:633–40. https://doi.org/10.1002/andp.19103360310.
[7] Knudsen M. The kinetic theory of gases. London: Methuen & Co., Ltd.; 1934.
[8] Pollard WG, Present RD. On gaseous self-diffusion in long capillary tubes. Phys Rev 1948;73:762–74. https://doi.org/10.1103/PhysRev. 73.762.
[9] Guo L, Chen S, Robbins MO. Effective slip boundary conditions for sinusoidally corrugated surfaces. Phys Rev Fluids 2016;1:74102. https://doi.org/10.1103/PhysRevFluids. 1.074102.
[10] Dushman S, Brown SC. Scientific foundations of vacuum technique. Am J Phys 1962;30. https://doi.org/10.1119/1.1942137. 612–612.
[11] Wleklinski JJ. A calculation of gaseous slip velocity and microscale flow fields from a molecular-continuum matching analysis. Phys A Stat Mech Its Appl 2001;291:197–210. https://doi.org/10.1016/S0378-4371(00)00507-0.
[12] Wu P, Nikolov A, Wasan D. Capillary dynamics driven by molecular self-layering. Adv Colloid Interface Sci 2017;243:114–20. https://doi.org/10.1016/J.CIS.2017.02.004.
[13] Kogan MN. Kinetic theory in aerothermodynamics. Prog Aerosp Sci 1992;29:271–354. https://doi.org/10.1016/0376-0421(92)90007-5.
[14] Ho C, Tai Y. Micro-electro-mechanical-systems (MEMS) and fluid flows. Annu Rev Fluid Mech 1998;30:579–612. https://doi.org/10.1146/annurev.fluid.30.1.579.
[15] Wu P, Nikolov AD, Wasan DT. Capillary rise: validity of the dynamic contact angle models. Langmuir 2017;33:7862–72. https://doi.org/10.1021/acs.langmuir.7b01762.
[16] Wang FP, Pore Reed RM. Networks and fluid flow in gas shales. Soc Petroleum Eng 2009. https://doi.org/10.2118/124253-MS.
[17] Wang L, Zeng Z, Zhang L, Qiao L, Zhang Y, Lu Y. A new boundary scheme for simulation of gas flow in kerogen pores with considering surface diffusion effect. Phys A Stat Mech Its Appl 2018;495:180–90. https://doi.org/10.1016/J.PHYSA.2017.12.028.
[18] Fathi E, Tinni A, Akkutlu IY. Correction to Klinkenberg slip theory for gas flow in nano-capillaries. Int J Coal Geol 2012;103:51–9. https://doi.org/10.1016/J.COAL.2012.06.008.
[19] Ashrafi Moghadam A, Chalaturnyk R. Expansion of the Klinkenberg's slippage equation to low permeability porous media. Int J Coal Geol 2014;123:2–9. https://doi.org/10.1016/J.COAL.2013.10.008.
[20] Wang L, Tian Y, Yu X, Wang C, Yao B, Wang S, et al. Advances in improved/enhanced oil recovery technologies for tight and shale reservoirs. Fuel 2017;210:425–45. https://doi.org/10.1016/J.FUEL.2017.08.095.
[21] Wang S, Winterfeld PH, Wu Y-S. An efficient adaptive nonlinearity elimination preconditioned inexact newton method for parallel simulation of thermal-hydraulic-mechanical processes in fractured reservoirs. SPE Reserv. Simul. Symp., Society of Petroleum Engineers; 2015. doi: 10.2118/173227-MS.
[22] Oran ES, Oh CK, Cybyk BZ. Direct simulation Monte Carlo: recent advances and applications. Annu Rev Fluid Mech 1998;30:403–41. https://doi.org/10.1146/annurev.fluid.30.1.403.
[23] Kroese DP, Brereton T, Taimre T, Botev ZI. Why the Monte Carlo method is so important today. Wiley Interdiscip Rev Comput Stat 2014;6:386–92. https://doi.org/10.1002/wics.1314.
[24] Bird GA, A. G. Molecular gas dynamics. vol. 76. Oxford: 1976.
[25] Bird GA, A. G. Monte-Carlo simulation in an engineering context. Rarefied Gas Dyn Int Symp 12th, Charlottesville, VA, July 7-11, 1980, Tech Pap Part 1 (A82-13026 03-77) New York, Am Inst Aeronaut Astronaut 1981, P 239-255 1981;74:239–55.
[26] Bird GA. Recent advances and current challenges for DSMC. Comput Math with Appl 1998;35:1–14. https://doi.org/10.1016/S0898-1221(97)00254-X.
[27] Pan LS, Liu GR, Lam KY. Determination of slip coefficient for rarefied gas flows using direct simulation Monte Carlo. J Micromech Microeng 1999;9:89–96. https://doi.org/10.1088/0960-1317/9/1/312.
[28] Ho TA, Criscenti LJ, Wang Y. Nanostructural control of methane release in kerogen and its implications to wellbore production decline. Sci Rep 2016;6:28053. https://doi.org/10.1038/srep28053.
[29] He X, Luo L-S. Theory of the lattice Boltzmann method: from the Boltzmann equation to the lattice Boltzmann equation. Phys Rev E 1997;56:6811–7. https://

doi.org/10.1103/PhysRevE.56.6811.
[30] Chen S, Doolen GD. Lattice Boltzmann method for fluid flows. Annu Rev Fluid Mech 1998;30:329–64. https://doi.org/10.1146/annurev.fluid.30.1.329.
[31] Li Q, He Y, Tang G, Tao W. Lattice Boltzmann modeling of microchannel flows in the transition flow regime. Microfluid Nanofluidics 2011.
[32] Nie X, Doolen GD, Chen S. Lattice-Boltzmann simulations of fluid flows in MEMS. J Stat Phys 2002;107:279–89. https://doi.org/10.1023/A:1014523007427.
[33] Tang GH, Tao WQ, He YL. Gas slippage effect on microscale porous flow using the lattice Boltzmann method. Phys Rev E 2005;72:56301. https://doi.org/10.1103/PhysRevE.72.056301.
[34] Silva G, Semiao V. Consistent lattice Boltzmann modeling of low-speed isothermal flows at finite Knudsen numbers in slip-flow regime: application to plane boundaries. Phys Rev E 2017;96:13311. https://doi.org/10.1103/PhysRevE.96.013311.
[35] Li J. Direct Simulation method based on BGK equation. AIP Conf. Proc., vol. 1333, American Institute of Physics; 2011, p. 283–8. doi: 10.1063/1.3562662.
[36] Li J, Sultan AS. Klinkenberg slippage effect in the permeability computations of shale gas by the pore-scale simulations. J Nat Gas Sci Eng 2017;48:197–202. https://doi.org/10.1016/J.JNGSE.2016.07.041.
[37] Xu K. A gas-kinetic BGK scheme for the Navier-Stokes equations and its connection with artificial dissipation and Godunov method. J Comput Phys 2001;171:289–335. https://doi.org/10.1006/JCPH.2001.6790.
[38] Xu K. A well-balanced gas-kinetic scheme for the shallow-water equations with source terms. J Comput Phys 2002;178:533–62. https://doi.org/10.1006/JCPH.2002.7040.
[39] Liu H, Cao Y, Chen Q, Kong M, Zheng L. A conserved discrete unified gas kinetic scheme for microchannel gas flows in all flow regimes. Comput Fluids 2018;167:313–23. https://doi.org/10.1016/J.COMPFLUID.2018.03.023.
[40] Ohwada T, Xu K. The kinetic scheme for the full-Burnett equations. J Comput Phys 2004;201:315–32. https://doi.org/10.1016/j.jcp.2004.05.017.
[41] Xu K. Super-Burnett solutions for Poiseuille flow. Phys Fluids 2003;15:2077–80. https://doi.org/10.1063/1.1577564.
[42] Myong RS. Thermodynamically consistent hydrodynamic computational models for high-Knudsen-number gas flows. Phys Fluids 1999;11:2788. https://doi.org/10.1063/1.870137.
[43] Balakrishnan R. An approach to entropy consistency in second-order hydrodynamic equations. J Fluid Mech 2004;503:201–45. https://doi.org/10.1017/S0022112004007876.
[44] Grad H. On the kinetic theory of rarefied gases. Commun Pure Appl Math 1949;2:331–407. https://doi.org/10.1002/cpa.3160020403.
[45] Lockerby DA, Reese JM, Gallis MA. The usefulness of higher-order constitutive relations for describing the Knudsen layer. Phys Fluids 2005;17:100609https://doi.org/10.1063/1.1897005.
[46] Dinler A, Barber RW, Emerson DR, Stefanov SK, Orucoglu K. On the degree of boundary slip over nonplanar surfaces. Microfluid Nanofluidics 2013;15:807–16. https://doi.org/10.1007/s10404-013-1183-z.
[47] Vo TQ, Barisik M, Kim B. Near-surface viscosity effects on capillary rise of water in nanotubes. Phys Rev E 2015;92:53009. https://doi.org/10.1103/PhysRevE.92.053009.
[48] Deng S, Jiang R, Karimi-Fard M, Aydin A. Fluid-flow effects of compartmentalized distribution of compaction bands in an aeolian sandstone in three dimensions. Pet Geosci 2017;23:223–30. https://doi.org/10.1144/petgeo2016-051.
[49] Ho TA, Wang Y, Xiong Y, Criscenti LJ. Differential retention and release of CO2 and CH4 in kerogen nanopores: implications for gas extraction and carbon sequestration. Fuel 2018;220:1–7. https://doi.org/10.1016/J.FUEL.2018.01.106.
[50] Wu K, Li X, Wang C, Yu W, Chen Z. Model for surface diffusion of adsorbed gas in nanopores of shale gas reservoirs. Ind Eng Chem Res 2015;54:3225–36. https://doi.org/10.1021/ie504030v.
[51] Shi Y, Lee YT, Kim AS. Knudsen diffusion through cylindrical tubes of varying radii: theory and Monte Carlo simulations. Transp Porous Media 2012;93:517–41. https://doi.org/10.1007/s11242-012-9966-3.
[52] Wu L, Liu H, Reese JM, Zhang Y. Non-equilibrium dynamics of dense gas under tight confinement. J Fluid Mech 2016;794:252–66. https://doi.org/10.1017/jfm.2016.173.
[53] Wu K, Chen Z, Li X, Xu J, Li J, Wang K, et al. Flow behavior of gas confined in nanoporous shale at high pressure: real gas effect. Fuel 2017;205:173–83. https://doi.org/10.1016/J.FUEL.2017.05.055.
[54] Wu K, Chen Z, Li X, Guo C, Wei M. A model for multiple transport mechanisms through nanopores of shale gas reservoirs with real gas effect–adsorption-mechanic coupling. Int J Heat Mass Transf 2016;93:408–26. https://doi.org/10.1016/J.IJHEATMASSTRANSFER.2015.10.003.
[55] Song W, Yao J, Li Y, Sun H, Zhang L, Yang Y, et al. Apparent gas permeability in an organic-rich shale reservoir. Fuel 2016;181:973–84. https://doi.org/10.1016/J.FUEL.2016.05.011.
[56] Yang Y, Yao J, Wang C, Gao Y, Zhang Q, An S, et al. New pore space characterization method of shale matrix formation by considering organic and inorganic pores. J Nat Gas Sci Eng 2015;27:496–503. https://doi.org/10.1016/J.JNGSE.2015.08.017.
[57] Cercignani C. higher order slip according to the linearized Boltzmann equation. 1964.
[58] Hadjiconstantinou NG. Comment on Cercignani's second-order slip coefficient. Phys Fluids 2003;15:2352. https://doi.org/10.1063/1.1587155.
[59] Beskok A, Karniadakis G. A model for flows in channels, pipes, and ducts at micro and nano scales. Microscale Thermophys Eng 1999:3.
[60] Wu L, Bogy DB. New first and second order slip models for the compressible Reynolds equation. J Tribol 2003;125:558. https://doi.org/10.1115/1.1538620.
[61] Wu L. A slip model for rarefied gas flows at arbitrary Knudsen number. Appl Phys Lett 2008;93:1–4. https://doi.org/10.1063/1.3052923.
[62] Zhang WM, Meng G, Wei X. A review on slip models for gas microflows. Microfluid Nanofluidics 2012;13:845–82. https://doi.org/10.1007/s10404-012-1012-9.
[63] Wang L, Wang S, Zhang R, Wang C, Xiong Y, Zheng X, et al. Review of multi-scale and multi-physical simulation technologies for shale and tight gas reservoirs. J Nat Gas Sci Eng 2017;37:560–78. https://doi.org/10.1016/j.jngse.2016.11.051.
[64] Wang S, Lukyanov AA, Wang L, Wu Y-S, Pomerantz A, Xu W, et al. A non-empirical gas slippage model for low to moderate Knudsen numbers. Phys Fluids 2017;29:12004. https://doi.org/10.1063/1.4974319.
[65] Wang S, Pan Z, Zhang J, Yang Z, Wang Y, Wu Y-S, et al. On the Klinkenberg effect of multicomponent gases. Proc. – SPE Annu. Tech. Conf. Exhib., 2017.
[66] Li Q, He YL, Tang GH, Tao WQ. Lattice Boltzmann modeling of microchannel flows in the transition flow regime. Microfluid Nanofluidics 2011;10:607–18. https://doi.org/10.1007/s10404-010-0693-1.
[67] Colin S, Lalonde P, Caen R. Validation of a second-order slip flow model in rectangular microchannels. Heat Transf Eng 2004;25:23–30. https://doi.org/10.1080/01457630490280047.
[68] Loyalka SK. Velocity slip coefficient and the diffusion slip velocity for a multicomponent gas mixture. Phys Fluids 1971;14:2599. https://doi.org/10.1063/1.1693380.
[69] Naris S, Valougeorgis D, Kalempa D, Sharipov F. Gaseous mixture eow between two parallel plates in the whole range of the gas rarefaction n.d. doi: 10.1016/j.physa.2003.12.047.
[70] Takata S. Diffusion slip for a binary mixture of hard-sphere molecular gases: numerical analysis based on the linearized Boltzmann equation. AIP Conf. Proc., vol. 585, AIP; 2001, p. 22–9. doi: 10.1063/1.1407538.
[71] Garcia RDM, Siewert CE. The viscous-slip, diffusion-slip, and thermal-creep problems for a binary mixture of rigid spheres described by the linearized Boltzmann equation. Eur J Mech – B/Fluids 2007;26:749–78. https://doi.org/10.1016/J.EUROMECHFLU.2006.12.002.
[72] Sharipov F, Kalempa D. Velocity slip and temperature jump coefficients for gaseous mixtures. I. Viscous slip coefficient. Phys Fluids 2003;15:1800. https://doi.org/10.1063/1.1574815.
[73] Sharipov F, Kalempa D. Velocity slip and temperature jump coefficients for gaseous mixtures. II. Thermal slip coefficient. Phys Fluids 2004;16:759–64. https://doi.org/10.1063/1.1644572.
[74] Sharipov F, Kalempa D. Velocity slip and temperature jump coefficients for gaseous mixtures. III. Diffusion slip coefficient. Phys Fluids 2004;16:3779–85. https://doi.org/10.1063/1.1781159.
[75] Sharipov F, Kalempa D. Velocity slip and temperature jump coefficients for gaseous mixtures. IV. Temperature jump coefficient. Int J Heat Mass Transf 2005;48:1076–83. https://doi.org/10.1016/J.IJHEATMASSTRANSFER.2004.09.035.
[76] Sharipov F, Gramani Cumin LM, Kalempa D. Plane Couette flow of binary gaseous mixture in the whole range of the Knudsen number. Eur J Mech – B/Fluids 2004;23:899–906. https://doi.org/10.1016/J.EUROMECHFLU.2004.03.002.
[77] Hyakutake T, Yamamoto K, Takeuchi H. Flow of Gas Mixtures through Micro Channel. AIP Conf. Proc., vol. 762, AIP; 2005, p. 780–8. doi: 10.1063/1.1941630.
[78] Arcidiacono S, Karlin IV, Mantzaras J, Frouzakis CE. Lattice Boltzmann model for the simulation of multicomponent mixtures. Phys Rev E 2007;76:46703. https://doi.org/10.1103/PhysRevE.76.046703.
[79] Bentz JA, Tompson RV, Loyalka SK. Viscosity and velocity slip coefficients for gas mixtures: Measurements with a spinning rotor gauge. J Vac Sci Technol A Vacuum, Surfaces, Film 1999;17:235. https://doi.org/10.1116/1.581577.
[80] Yamaguchi H, Takamori K, Perrier P, Graur I, Matsuda Y, Niimi T. Viscous slip coefficients for binary gas mixtures measured from mass flow rates through a single microtube. Phys Fluids 2016;28:92001. https://doi.org/10.1063/1.4961647.
[81] Kennard E. Kinetic theory of gases. 1st ed. New York and London: McGraw-Hill Book Co; 1938.
[82] Bennett HE, Porteus JO. Relation between surface roughness and specular reflectance at normal incidence. J Opt Soc Am 1961;51:123. https://doi.org/10.1364/JOSA.51.000123.
[83] Davies H. The reflection of electromagnetic waves from a rough surface. Proc IEE – Part IV Inst Monogr 1954;101:209–14. https://doi.org/10.1049/pi-4.1954.0025.
[84] Harvey JE, Schröder S, Choi N, Duparré A. Total integrated scatter from surfaces with arbitrary roughness, correlation widths, and incident angles. Opt Eng 2012;51:13402. https://doi.org/10.1117/1.OE.51.1.013402.
[85] Shen C, Fan J, Xie C. Statistical simulation of rarefied gas flows in micro-channels. J Comput Phys 2003;189:512–26. https://doi.org/10.1016/S0021-9991(03)00231-6.
[86] Maurer J, Tabeling P, Joseph P. Second-order slip laws in microchannels for helium and nitrogen. Phys Fluids (1994- 2003;15:2613–21. https://doi.org/10.1063/1.1599355.
[87] Yampolskii Y, Pinnau I, Freeman B. Materials science of membranes for gas and vapor separation. 1st ed. John Wiley & Sons; 2006.
[88] Reid RC, Prausnitz JM, Sherwood TK, Thomas K, 1903-1976. The properties of

gases and liquids. McGraw-Hill; 1977.
[89] Law CK. Combustion physics. 1st ed. Cambridge University Press; 2006.
[90] Long Y, Palmer JC, Coasne B, Śliwinska-Bartkowiak M, Gubbins KE. Under pressure: quasi-high pressure effects in nanopores. Microporous Mesoporous Mater 2012;154:19–23. https://doi.org/10.1016/J.MICROMESO.2011.07.017.
[91] Barisik M, Beskok A. Scale effects in gas nano flows. Phys Fluids 2014;26:52003. https://doi.org/10.1063/1.4874678.
[92] Wu K, Chen Z, Li J, Li X, Xu J, Dong X. Wettability effect on nanoconfined water flow. Proc Natl Acad Sci USA 2017;114:3358–63. https://doi.org/10.1073/pnas.1612608114.
[93] Zerpa L, Gao F, Wang S. An analytical solution and numerical modeling study of gas hydrate saturation effects on porosity and permeability of porous media. Am. Geophys. Union, Fall Meet. 2017, 2017.
[94] Wang S, Pomerantz AE, Xu W, Lukyanov A, Kleinberg RL, Wu Y-S. The impact of kerogen properties on shale gas production: a reservoir simulation sensitivity analysis. J Nat Gas Sci Eng 2017:48. https://doi.org/10.1016/j.jngse.2017.06.009.